Solvent Polarity and Framework Hydrophobicity of Hf-BEA Zeolites Influence Aldol Addition Rates in Organic Media

Alexander A. Khechfe, Thaïs B. M. Matha, and Yuriy Román-Leshkov*

Cite This: *ACS Catal.* 2023, 13, 6474−6485

Read Online

ACCESS | Metrics & More | Article Recommendations | Supporting Information

ABSTRACT: Solvent identity and pore polarity are known to influence Lewis acidic catalysis in zeolite pores for a variety of liquid-phase chemistries. We investigated how these parameters alter the rates of self-aldol addition of ethyl pyruvate (EP), a model biomass-derived compound, over hydrophobic and hydrophilic Hf-BEA zeolites in both toluene and acetonitrile solvents. Aldol addition rates are of first order across the entire EP activity range (0.02−0.4) for all four systems, consistent with the nucleophilic attack by the enolate as the rate-determining step and a single adsorbed EP as the most abundant reactive intermediate. Apparent first-order rate constants span 2 orders of magnitude across the four systems; at 363 K, the highest rates were observed over

hydrophobic Hf-BEA-F in toluene (k_{app} = 0.36 (mmol) (mmol closed Hf)$^{-1}$ (s)$^{-1}$), while the lowest rates were observed in hydrophilic Hf-BEA-OH in an acetonitrile solvent (k_{app} = 0.0026 (mmol) (mmol closed Hf)$^{-1}$ (s)$^{-1}$). Apparent reaction enthalpies and entropies for each system, estimated using non-ideal transition-state theory, revealed that despite the substantial rate constant variation across the four systems, apparent enthalpies for Hf-BEA-F in both solvents and Hf-BEA-OH in acetonitrile were within the error of each other (∼70 kJ mol^{-1}). Reactions performed using Hf-BEA-OH with toluene featured a higher apparent enthalpic barrier of 83.8 kJ mol^{-1}. The differences between the systems are attributed to hydrogen-bonding interactions between the EP molecules and polar silanol nests during catalysis in toluene using Hf-BEA-OH, which hinder EP adsorption to the active site in the hydrophilic framework. These hydrogen-bonding interactions are not present when acetonitrile is used as the solvent, as acetonitrile itself binds to and blocks silanol groups. Equilibrium EP absorption measurements indicate that while both toluene and acetonitrile are present in pores during catalysis, neither solvent forms a tight solvation shell around EP in the pores that must be disrupted prior to EP adsorption. These findings show that aldol addition kinetics are not significantly modified by solvent polarity in hydrophobic frameworks beyond site-blocking effects; however, silanol nests in hydrophilic frameworks significantly alter substrate adsorption to the active site.

KEYWORDS: *zeolites, aldol condensation, solvent effects, hydrophobicity, kinetics, biomass upgrading, Hf-BEA*
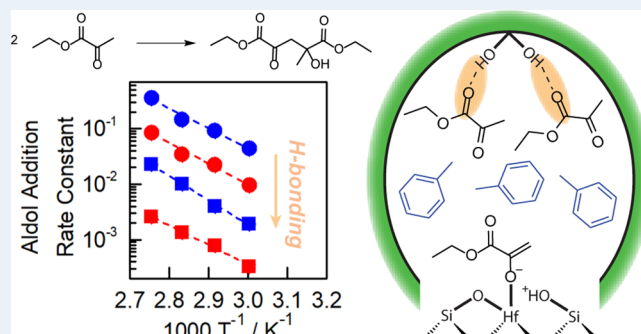
INTRODUCTION

Aldol condensation is a versatile carbon−carbon coupling reaction for biomass upgrading schemes that require elongation of the carbon backbone while increasing the carbon to oxygen ratio for the production of fuels, monomers, or platform chemicals.[1−6] In this reaction, C−C bonds are formed between a pair of carbonyl groups possessing at least one reactive α-hydrogen via the nucleophilic attack of a carbonyl by an enolate intermediate in the presence of an acid or a base catalyst.[3] Aldol condensation reactions are commonly catalyzed by strong homogeneous bases, such as hydroxides, alkoxides, and amides,[7,8] or by solid bases, such as alkali or alkaline-earth oxides.[2,9−11] In a typical base-catalyzed system, the enolate is formed by direct deprotonation of the α-hydrogen. An alternative mechanism is that of soft enolization, which uses a Lewis acid and Brønsted base pair to perform this activation under milder conditions. Specifically, as the carbonyl

adsorbs onto the Lewis acid site, the acidity of the α-H increases and ultimately becomes more adept at undergoing deprotonation by the adjacent Brønsted base. Soft enolization is a common mechanism in type II aldolases and can be performed with high specificity over a variety of substrates, including those that are incompatible with strong bases (e.g., keto acids).[12,13] It is therefore valuable to develop inorganic analogues that mimic the soft enolization pathways.

Lewis acidic zeolites containing tetravalent heteroatoms, such as Ti, Zr, Hf, or Sn, are versatile catalysts for the

Scheme 1. EP Aldol Addition Reaction to Diethyl 2-Hydroxy-2-methyl-4-oxopentanedioate ((EP)₂OH), followed by Dehydration to Dehydrated Diester Products

Ethyl Pyruvate
(EP)

Diethyl 2-hydroxy-2-methyl
-4-oxopentanedioate
((EP)₂OH)

Dehydrated
Diesters
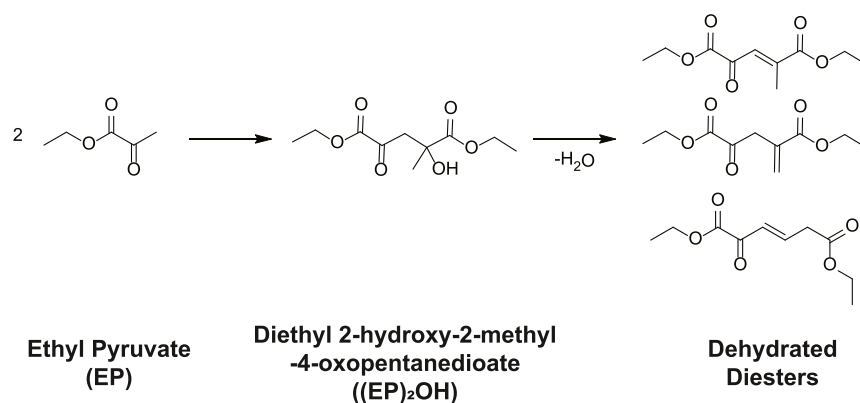
activation of oxygenates.[14−23] Zeolites additionally offer several tunable features, including the pore size,[24−26] hydrophobicity/polarity,[27−29] and active site center,[30−32] allowing for extensive control of the active site environment. Due to their ability to selectively control reaction environments via transition-state stabilization and solvent structure, Lewis acidic zeolites are often proposed as biomimetic catalysts that carry many of the same advantages as enzyme catalysts.[33] Indeed, Lewis acidic zeolites have been shown to be active aldol condensation catalysts.[34−38]

Lewis et al. reported that acid−base pairs in Sn-BEA zeolites are capable of soft enolization, where the framework oxygen adjacent to the metal heteroatom acts as a Brønsted base that can abstract the α-proton and form a silanol group and an adsorbed enolate intermediate.[39] This process is facilitated by the transfer of electron density from the metal center to adjacent framework oxygens and the delocalization of the catalyst LUMO.[31,40] After adsorption of a second carbonyl to the same active site, a C−C bond can be formed via a nucleophilic attack on the second carbonyl by the enolate. The resulting intermediate is then protonated by the silanol group and can desorb as the aldol addition product. Subsequent dehydration on an acid site completes the aldol condensation pathway.

Since these materials are acidic, they can activate substrates with acid functional groups that would otherwise deactivate over a base. Additionally, confining the reaction to a <1 nm diameter pore prevents potentially unfavorable double aldol condensations and improves selectivity toward desired single aldol products.[39] Previous studies have shown that the choice of the heteroatom greatly influences the activity of a Lewis acidic zeolite for aldol condensation.[37,41] Wang et al. studied different catalysts for the self-aldol condensation of ethyl pyruvate (EP) and concluded that Hf-BEA and Zr-BEA had higher rates than Sn-BEA, while all catalysts studied had comparable selectivities of 60−70%.[37]

Gas-phase aldol condensation studies with these materials have provided excellent insight into the nature of this reaction. Zhang et al. studied the effect of Ti-BEA framework polarity for gas-phase acetaldehyde (CH₃CHO) aldol condensation and esterification and observed that aldol condensation rates are first-order in CH₃CHO (0.05−1 kPa CH₃CHO). No kinetic isotope effect was seen when CD₃CHO was substituted for CH₃CHO, indicating that the nucleophilic attack of the enolate on a second adsorbed carbonyl, not enolate formation, is kinetically relevant for aldol condensation on these

materials.[38] Observed rates were fivefold greater in the most hydrophilic Ti-BEA than in hydrophobic, defect-free Ti-BEA. The increase in rate with silanol density was attributed to the presence of adsorbed ethoxy groups on silanol nests that favorably modify the electric field around the active site. Gas-phase acetaldehyde aldol condensation has been studied extensively over anatase TiO₂, with reports of either enolate formation[42] or nucleophilic attack[43] as the rate-limiting step. In the case where nucleophilic attack is kinetically relevant, the TiO₂ surface is covered predominantly with unreactive ethanol intermediates that prevent the formation of reactive enolate−acetaldehyde pairs by blocking active sites. When TiO₂ surfaces are sparsely populated, enolate formation becomes rate-determining. The introduction of an *n*-heptane liquid phase during gas-phase acetone aldol condensation over anatase TiO₂ was found to increase rates by up to 2.5× via stabilization of the enolate intermediate and decrease deactivation rate constants by an order of magnitude, indicating that the presence of a solvent can significantly affect aldol condensation kinetics.[44]

While Lewis acidic zeolites are understood to be excellent liquid-phase aldol addition catalysts, a detailed kinetic study using non-aqueous solvents that elucidates the role of the solvent and framework polarity has not yet been performed. Indeed, pore and solvent polarity have been shown to significantly affect reaction kinetics in microporous catalysts for a variety of reactions. Bregante et al. studied alkene epoxidation with H₂O₂ over Ti-BEA zeolites and observed that the most hydrophilic zeolite gave the highest selectivities and epoxidation turnover rates despite similar H₂O₂ decomposition rates across all Ti-BEA samples.[45] The apparent activation entropy is increased when water clusters anchored to silanol nests ((SiOH)₄) near the active sites are disrupted. Turnover rates also increased by 20× in the presence of water for the most hydrophilic Ti-BEA, with no significant change for hydrophobic Ti-BEA. In contrast, glucose isomerization rates were sixfold higher for Ti-BEA-F than Ti-BEA-OH in zero- and first-order kinetic regimes due to entropic stabilization of the transition state in hydrophobic pores, despite a small enthalpic stabilization in hydrophilic pores.[46] Meerwein−Ponndorf−Verley reduction and Oppenauer oxidation (MPVO) between 2-butanol and cyclohexanone was observed to have turnover rates 10-fold higher in hydrophobic Sn-BEA-F than hydrophilic Sn-BEA-OH.[47] This difference in rates was attributed to entropic release upon rupturing of ordered hydrogen-bonded 2-butanol networks upon cyclohexanone

adsorption in Sn-BEA-F, whereas no such ordered networks were present in Sn-BEA-OH.

Here, we studied the effect of framework hydrophobicity and solvent polarity on self-aldol addition rates of EP to diethyl 2-hydroxy-2-methyl-4-oxopentanedioate (($EP)_2OH$) and its dehydrated diesters (Scheme 1) over Hf-BEA zeolites. This reaction was investigated previously in our group[37] as a promising pathway to generate substituted di-acid monomers for the production of renewable polyesters. Aldol addition turnover rates (normalized per Lewis acidic Hf site) were measured on Hf-BEA-F and Hf-BEA-OH in non-polar toluene and polar acetonitrile solvents as functions of temperature (333−363 K) and EP activity (0.02−0.4). Rate constants obtained through initial rate measurements were used to extract apparent activation enthalpies and entropies that aid in understanding the environment around the active site during catalysis. These rate measurements showed that EP adsorption and self-aldol addition rates can be modified by combinations of the framework polarity and solvent, giving another handle for rate control beyond active site identity.

■ EXPERIMENTAL METHODS

Catalyst Synthesis. Hf-BEA-F with a Si/Hf ratio of 327 was prepared using a fluoride-mediated hydrothermal synthesis procedure, as reported previously.[37] An aqueous tetra-ethyl ammonium hydroxide (TEAOH; 13.366 g, 40 wt %, Sigma-Aldrich) solution was added to a perfluoroalkoxyalkane (PFA, Savillex) jar containing a polytetrafluoroethylene (PTFE, VWR) stir bar. Tetraethyl orthosilicate (TEOS; 12.107 g, 99 wt %, Sigma-Aldrich) was then added to the solution and stirred for 90 min. $HfCl_4$ (0.063 g, Sigma-Aldrich) was added to ethanol (1.997 g, 99.5 wt %, Koptec) in a centrifuge tube and vortexed until dissolved, then added to the jar to give a Si/Hf ratio of 300 in the initial gel. The mixture was then stirred in a fume hood overnight to evaporate ethanol and excess water. Hydrofluoric acid (1.295 g, 48 wt %, Sigma-Aldrich) was added dropwise, and the mixture was stirred with a PTFE spatula. The final molar composition of the gel was 1 SiO_2: 0.0033 $HfCl_4$: 0.55 TEAOH: 0.54 HF: 7.5 H_2O. Dealuminated BEA zeolite (0.173 g) was then added to the mixture as a seed, which was transferred to a 45 mL PTFE lined, stainless-steel autoclave and heated to 413 K under 40 rpm rotation for 20 days. The product was then recovered by centrifugation, washed with DI water and acetone, and dried in an oven at 373 K. The dry powder was then calcined at 423 K for 2 h and 853 K for 6 h (1 K min⁻¹ ramp) under 100 cm³ min⁻¹ of dry flowing air. Other reported Hf-BEA samples were prepared and characterized previously using similar methods with different $HfCl_4$ precursor masses.[48] Si-BEA-F samples were prepared previously using a similar procedure, except for the omission of $HfCl_4$ and a crystallization time of 7 days instead of 20.[14,37]

Dealuminated BEA was prepared by the addition of Al-BEA (2.55 g, Si/Al = 12.5, CP814E, Zeolyst) to concentrated nitric acid (250 cm³, 70 wt %, Sigma-Aldrich) in a 500 mL round-bottom flask with a stir bar and a condenser attachment.[48,49] The flask was heated in a metal bead bath to 353 K and stirred for 24 h at 500 rpm. After cooling, the solids were recovered via centrifugation and washed with DI water until the pH values between washes did not change. The solids were then dried at 373 K overnight in an oven and then calcined at 423 K for 2 h and 853 K for 6 h (1 K min⁻¹ ramp) under 100 cm³ min⁻¹ dry flowing air.

Hf-BEA-OH with a Si/Hf ratio of 145 was prepared via postsynthetic grafting of Hf into the dealuminated BEA sample. Dealuminated BEA (∼1 g) and a PTFE stir bar were placed into a 500 cm³ two-neck round-bottom flask. A glass stopper was used to seal one opening, and the other was connected to a Schlenk line via a reflux condenser. The dealuminated BEA samples were then dehydrated overnight at 623 K under dynamic vacuum, cooled to room temperature, and held under a dry N_2 purge. The glass stopper was then removed from the round-bottom flask, and 130 mL of acetonitrile (Sigma-Aldrich) was added to the dried deal-uminated BEA while stirring at 500 rpm. $HfCl_4$ (0.033 g, Sigma-Aldrich) was then dissolved in ∼10 mL of acetonitrile and added to the flask. Acetonitrile used for this synthesis was not rigorously dried (see the Catalyst Characterization section of the Results and Discussion). The flask was then resealed and stirred under acetonitrile reflux (356 K) overnight. The solids were then recovered via centrifugation, washed with acetone and water, dried in an oven at 373 K overnight, and then calcined at 423 K for 2 h and 853 K for 6 h (1 K min⁻¹ ramp) under 100 cm³ min⁻¹ dry flowing air. Other Hf-BEA-OH samples reported were prepared using the same method with different amounts of $HfCl_4$ added.

Catalyst Characterization. Powder X-ray diffraction (PXRD) was used to determine the crystal structure of the zeolites. PXRD patterns were collected with a Bruker D8 diffractometer with a Cu Kα radiation source between 2θ = 3−50° and a scan rate of 0.077° s⁻¹. XRD patterns are shown in the Supporting Information.

Elemental analysis was performed by inductively coupled plasma mass spectrometry (ICP-MS) using an Agilent 7900 ICP-MS instrument. Approximately 10 mg of zeolite powder was added to a 15 mL polypropylene centrifuge tube and dissolved in 200 μL of hydrofluoric acid overnight prior to dilution with 2 wt % HNO_3 (Veritas Double Distilled, GFS Chemicals Inc.) to obtain approximately 100 ppb of metal in the final solution. Hf concentrations were determined from calibration curves prepared from standard solutions of 1000 ppm of Hf in 5% nitric acid and <0.5% hydrofluoric acid (TraceCERT, Sigma-Aldrich) diluted in 2 wt % HNO_3.

Fourier transform infrared spectroscopy (FTIR) spectra were acquired from 4000 to 400 cm⁻¹ using a Bruker Vertex 70 spectrophotometer with a Hg−Cd−Te (MCT) detector and cooled with liquid N_2 by averaging 128 scans at 1 cm⁻¹ resolution. The empty cell was heated to 673 K for 2 h under dynamic vacuum (<10⁻⁵ Torr, Edwards T-Station 75 Turbopump), and an IR spectrum of the empty cell was then measured at 303 K. Around 5 mg of the zeolite powder was pressed in a 7 mm diameter wafer, held in place using a stainless-steel sample holder (Harrick Scientific Products Inc.), and placed into a high-temperature transmission IR cell (Harrick Scientific Products Inc.) equipped with KBr windows (32 × 3 mm; Harrick Scientific Products Inc.). Dry N_2 was continuously flown into the space between the detector and the cell to remove residual traces of CO_2 and H_2O.

The pellet was heated to 423 K at a rate of 1 K min⁻¹ under 80 cm³ min⁻¹ of flowing dry air for 6 h. It was then cooled to 303 K while keeping the air flow, and finally, the cell was evacuated until a steady pressure below 8 × 10⁻⁵ Torr was obtained. A single scan was taken to obtain a parent spectrum of the sample prior to dosing of titrants. The experiment was performed with doses of ∼0.1−1.0 μmol of acetonitrile-d_3 (CD_3CN, anhydrous, >99.8 atom % D, Sigma-Aldrich) that

Table 1. Si/Hf Ratio, Framework Lewis Acid Sites per Total Hf Content, Open/Closed Acidic Hf Ratio, Number of SiOH Groups, and Edge Energy for the Hydrophobic and Hydrophilic Samples Used in This Study[a]

sample	Si/Hf	LAS/total Hf	open/closed ratio	SiOH content/μmol g^{-1}	edge energy/eV
Hf-BEA-F	327	0.92	0.74	45	4.06
	154	1.35	0.76	189	
	102	0.54	0.45	87	
Hf-BEA-OH	102	0.69	0.38	517	4.22
	145	1.04	0.30	1165	
	251	1.01	0.11	1061	
Si-BEA-F				58	
Si-BEA-OH				1581	

[a]Edge energies were obtained using UV−vis absorption, which can be found in Figure S4.

was previously purified by performing three successive freeze−pump−thaw cycles to remove dissolved gases. The pressure of the cell was measured using a Baratron capacitance manometer (0.01 Torr resolution; MKS Instruments). After 30 s of constant pressure, an IR spectrum was taken. Reported IR spectra were baseline-corrected and normalized by the total T-O-T peak area (2100−1750 cm^{-1}) from the pre-dose scan. Peak deconvolution to determine open Hf, closed Hf, and silanol counts was performed using algorithms our group has previously reported.[47,48]

Diffuse reflectance ultraviolet−visible (DRUV) spectra were measured on a Cary 5000 spectrometer (Agilent) with a DiffusIR diffuse reflectance accessory and environmental chamber (PIKE Technologies). Samples were dehydrated under flowing dry air for 2 h at 523 K (5 K min^{-1}) and then cooled to 303 K before scanning. Reflectance was converted to absorbance using the Kubelka−Munk function.

Measurement of Aldol Addition Kinetics in Hf-BEA. Aldol addition kinetic studies were performed in glass batch reactors (10 cm^3, VWR scientific). Prior to rate measurements, batch reactors were sonicated in acetone, ethanol, and deionized water for 30 min each and dried at 373 K. Each vial was filled with a PTFE-coated magnetic stir bar (VWR scientific) and 3−10 mg of Hf-BEA zeolite such that the ratio of EP to the Lewis acidic framework Hf was at least 40. The vial was then sealed with a PTFE-lined silicone septum with an aluminum crimp top (Supelco). Reactant solutions containing EP (Sigma-Aldrich, 99%) in toluene (Sigma-Aldrich, anhydrous 99.8%, equipped with a SureSeal) or acetonitrile (Sigma-Aldrich, HPLC Grade 99.9%, kept dry with 3A molecular sieves) with ∼0.5 mol % of o-xylene (Sigma-Aldrich, HPLC Grade, 98%) as an internal standard were added to a separate vial. EP concentrations ranged from 0.015−0.5 M in toluene and 0.015−0.25 M in acetonitrile. Total solution volumes were ∼2 cm^3. The liquid-containing vial was sealed with another crimp seal. For reaction times of less than 180 min, liquid-containing vials were then preheated for at least 15 min at the desired reaction temperature in a magnetically stirred (800 rpm) silicone oil bath. After preheating, the reaction mixture was transferred to the catalyst vial using a gas-tight syringe to begin the reaction. For reaction times greater than 180 min, only the vial containing the catalyst and stir bar was preheated. After the desired amount of time, the reaction vial was quenched in an ice bath, filtered through a 0.2 μm PTFE syringe filter (VWR), and injected into a gas chromatograph (7890A, Agilent Technologies) equipped with a 30 m HP-5MS column and a flame ionization detector. Products were identified using a GC−MS (7820A GC, 5977B MSD, Agilent Technologies) equipped with a 30 m Agilent HP-5MS UI

column. Initial aldol addition turnover rates at a given condition were calculated by extrapolating total aldol products produced per closed Hf to a zero reaction time. Measurements were taken at <5% product conversion and gave initial rates within ∼15% to those calculated from full transient reaction profiles (Section S2). Unless otherwise noted, rates are normalized per closed Hf site, with site counts determined via CD$_3$CN titration, and include the formation of both the aldol product (EP)$_2$OH and the dehydrated diesters (Scheme 1). Fitting of kinetic data was performed in Origin.

EP Absorption Isotherms in Si-BEA. Liquid-phase EP absorption isotherms were acquired to determine EP uptake as a function of EP activity in different solvents and frameworks.[50] Solutions of toluene or acetonitrile, EP, and o-xylene (internal standard) with EP ranges similar to those studied for kinetics were made and added to 20−80 mg of Si-BEA-F or Si-BEA-OH in 5 mL glass scintillation vials. The vial was allowed to sit undisturbed for 24 h at ambient conditions (∼298 K) to allow for equilibration. After 24 h, the supernatant liquid was removed using a glass pipette, filtered through a 0.2 μm PTFE syringe filter, and injected into a gas chromatograph to determine the change in EP concentration after equilibration. Any EP uptake value that was found to be negative (i.e., too small to measure experimentally) is reported as 0 mmol EP g$_{cat}$$^{-1}$.

RESULTS AND DISCUSSION

Catalyst Characterization. PXRD patterns of samples synthesized using hydrothermal synthesis confirmed the successful synthesis of the Hf-BEA-F framework based on the presence of peaks at 2θ values of 7.75 and 22.5° (Figures S1 and S2). ICP-MS was used to obtain the Si/Hf ratio in the framework (Table 1). Individual Hf-BEA samples are referred to by the notation Hf-BEA-H(X), where H denotes the hydrophobicity (F for hydrophobic and OH for hydrophilic) and X refers to the Si/Hf ratio. Typical post-synthetic grafting of transition metals (Ti, Sn, and Zr) into dealuminated zeolite frameworks requires rigorous drying of the solvent over 3A molecular sieves prior to the addition of metal precursors.[38,45,47,51] However, these procedures generally resulted in either poor incorporation of Hf into the sample and/or LAS/Hf ratios <0.25, consistent with the formation of large amounts of HfO$_x$ (Figure S3). Reproducible and consistently high Hf incorporation was obtained when the acetonitrile solvent was used as received without the inclusion of a drying step, with the de-Al-BEA samples dried as normal. We hypothesize that despite the tendency of HfCl$_4$ to oxidize in the presence of water to form HfO$_2$, trace amounts of water that may be present in ambient acetonitrile aid in either the full

dissolution of the HfCl$_4$ precursor in acetonitrile or in grafting the Hf^{4+} cation into silanol nests. While water was not deliberately added at any step of the synthesis, acetonitrile stored under ambient conditions in our laboratory contained approximately 240 ppm of water based on the Karl–Fischer titration. This highlights an important contrast between the synthesis of Hf-BEA-OH and other hydrophilic BEA frameworks, such as Ti-BEA-OH and Sn-BEA-OH, that all require rigorously anhydrous conditions for successful grafting of metal cations.

ICP-MS is insufficient to determine whether the Hf in the sample is associated with a framework open site that is coordinated to three lattice oxygens and one hydroxide ligand ((SiO$_3$)HfOH), a framework closed site that is coordinated to four framework oxygens ((SiO$_4$)Hf), or extraframework HfO$_x$. Previous work has shown that FTIR spectra of CD$_3$CN adsorbed on Hf-BEA can be used to differentiate between open and closed sites based on the different vibrational energies of the nitrile bond on the two sites.[48] The same technique has been employed for distinguishing between open and closed sites on the more widely characterized Sn-BEA.[52–54] At low CD$_3$CN coverages, open and closed sites are titrated first, corresponding to peaks at $\nu(C\equiv N)_{Open}$ = 2313 cm^{-1} and $\nu(C\equiv N)_{Closed}$ = 2308 cm^{-1}, respectively. At higher CD$_3$CN coverages, silanol groups ($\nu(C\equiv N)_{SiOH}$ = 2276 cm^{-1}) begin to saturate, followed by the appearance of a peak corresponding to physisorbed CD$_3$CN ($\nu(C\equiv N)_{phys}$ = 2266 cm^{-1}).[48,55]

Figure 1 shows FTIR spectra of Hf-BEA-F(327) (Figure 1a) and Hf-BEA-OH(145) (Figure 1b) during CD$_3$CN titration.
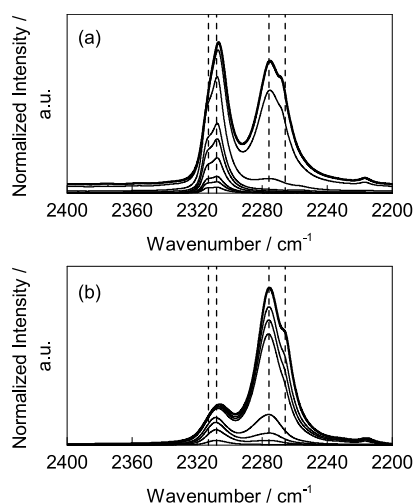

Figure 1. IR difference spectra (relative to spectra of the sample under vacuum after dehydration) of (a) Hf-BEA-F(327) and (b) Hf-BEA-OH(145) with increasing coverage of CD$_3$CN measured at 303 K. Dashed lines are expected $\nu(C\equiv N)$ stretching frequencies for CD$_3$CN chemisorbed to open Hf sites (2313 cm^{-1}), closed Hf sites (2308 cm^{-1}), and silanol groups (2275 cm^{-1}) as well as for physisorbed CD$_3$CN at 2265 cm^{-1}.

Open and closed sites begin to simultaneously saturate Hf-BEA-F(327), followed by saturation of silanol groups. The silanol peak at 2276 cm^{-1} is much larger in Hf-BEA-OH(145), indicating a much higher silanol density in the hydrophilic framework. Quantitative results of the Hf and silanol counts for these materials are found in Table 1.

Kinetics of EP Self-Aldol Addition in Hf-BEA-F and Hf-BEA-OH. Initial aldol addition rates were measured in triplicate on Hf-BEA-F(327) and Hf-BEA-OH(145) as functions of concentration in dry toluene and acetonitrile at temperatures of 333–363 K. Other Hf-BEA samples shown in Table 1 were used for controls. The results of these 288 independent batch reactions are shown in Figure 2. Turnover rates are described using thermodynamic activities due to expected non-ideal solution behavior that can affect reaction rates.[56] Activity coefficients (γ_i) were calculated using the UNIFAC group contribution method, and the activity of each species was calculated via

$$a_i = \frac{\gamma_i C_i}{C_i^0} \tag{1}$$

where C_i is the concentration of the component in mol L^{-1}, and C_i^0 is the concentration of the pure component.

Reaction kinetics measured on Hf-BEA were collected in a regime where turnover numbers were linear with reaction time (sample transient shown in Figure S6), indicating that rate measurements are not convoluted by equilibrium limitations and that deactivation is negligible under the timescales of these batch reactions. Rates were determined to be free of external or internal mass transfer artifacts (Figures S7 and S8).[57] The aldol addition rate per catalyst mass increased linearly with the moles of closed Hf per catalyst mass with the fitted trendline passing through the origin, indicating that aldol addition is predominantly catalyzed by closed sites and that the reaction does not proceed when the concentration of closed sites is zero (Figure S9). These findings are consistent with previous work showing that increasing loadings of open Sn sites on Sn-BEA do not correlate with increased reaction rates for the aldol addition of benzaldehyde and acetone and that other sites, likely closed Sn sites, were active for this reaction.[34] Thus, all reaction rates are normalized to the number of closed Hf sites, determined by CD$_3$CN titration, unless otherwise noted. Aldol addition resulted in the formation of the aldol product (EP)$_2$OH as well as three dehydrated diester isomers (GC–MS for each product are in Figures S10–S13). Generally, (EP)$_2$OH comprised >80% of the aldol products at EP activities above ~0.1 on Hf-BEA-F, with the moles of dehydrated products becoming more comparable to those of (EP)$_2$OH at lower EP activities (sample product distributions in Figure S14).

Going forward, each of the four solvent/framework systems will be referred to as Hf-BEA-H-S, where H refers to the hydrophobicity of the sample (F for hydrophobic and OH for hydrophilic), and S refers to the solvent (Tol for toluene or MeCN for acetonitrile). Regardless of solvent choice, observed rates (per closed Hf) were higher in Hf-BEA-F than in Hf-BEA-OH. For a given framework hydrophobicity, observed rates were higher in toluene than acetonitrile. Overall, rates decrease in the order of Hf-BEA-F-Tol > Hf-BEA-F-MeCN > Hf-BEA-OH-Tol > Hf-BEA-OH-MeCN, indicating inhibiting effects of the polar acetonitrile solvent and a more polar framework. We note that the lower aldol addition rates in the hydrophilic framework are in contrast to observations on gas-phase acetaldehyde condensation in Ti-BEA, which saw up to a fivefold increase in the aldol condensation rate as the silanol density was increased.[38]

To more quantitatively compare the kinetics across the four conditions, these data were fit to aldol addition rate
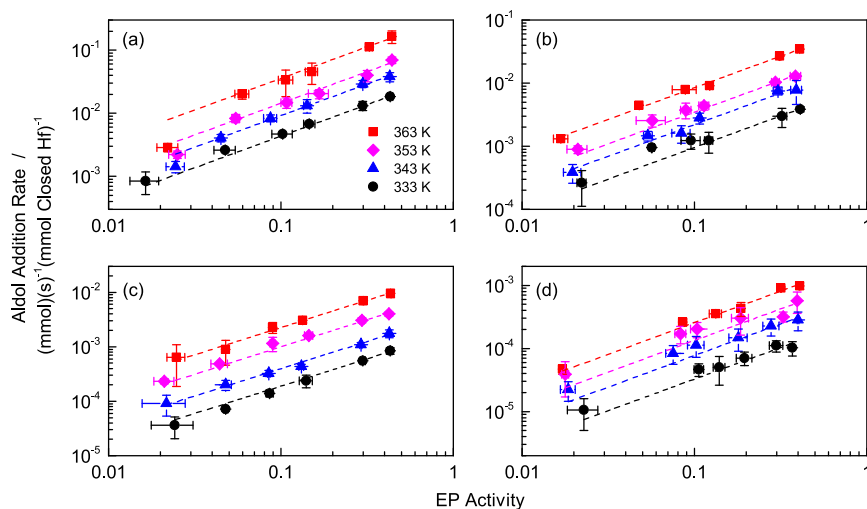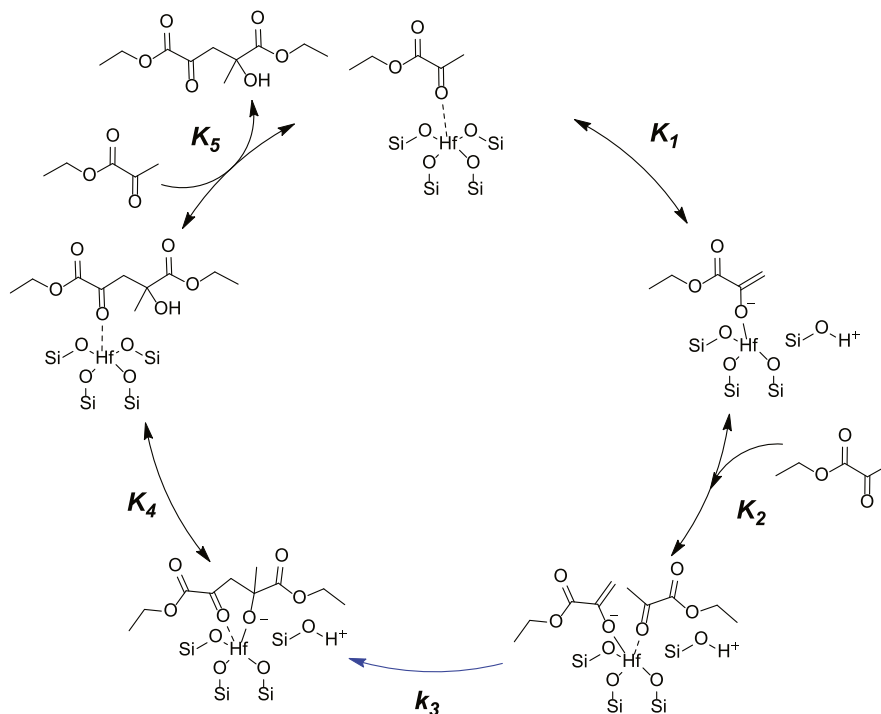
Figure 2. EP aldol addition rate (per closed Hf) vs a_{EP} in Hf-BEA-F(327) in (a) toluene and (b) acetonitrile and Hf-BEA-OH(145) in (c) toluene and (d) acetonitrile at 333−363 K as functions of EP activity. Each point represents the average of three independently run batch reactions, with error bars representing the standard deviation. Dashed lines are linear regressions of eq 3.

Scheme 2. EP Aldol Addition Mechanism over Hf-BEA[a]

[a]Hf sites are assumed to be always covered with an EP molecule, reaction intermediate, or coordinating solvent. Adsorbed EP is then deprotonated to form an enolate intermediate (step 1), followed by the adsorption of a second EP molecule from the solution to the active site (step 2). This step is followed by the rate-determining nucleophilic attack of the second EP molecule by the enolate to form a deprotonated alcohol (step 3). The deprotonated alcohol is then protonated (step 4) before desorbing and being replaced by another solution phase EP (step 5).

expressions. Aldol addition of aldehydes and ketones in Lewis acidic zeolites proceeds through a known mechanism,[38,44] shown in Scheme 2, beginning with an EP adsorbed to a closed Hf site (EP*). The EP* then undergoes deprotonation to form the adsorbed enolate (En*) in step 1, followed by adsorption of a second EP to the same Hf site, forming an adsorbed EP*−En* pair (P*). The second adsorbed EP then undergoes rate-determining nucleophilic attack by the adsorbed enolate in step 3, forming a carbon−carbon bond and an adsorbed deprotonated aldol adduct (DA*). The DA* species is then

protonated by the neighboring silanol in step 4 to form an adsorbed product (EP)$_2$OH* and desorbed in step 5 as (EP)$_2$OH while being replaced by another solution-phase EP. The (EP)$_2$OH product can then go on to be dehydrated on a silanol nest or a framework Hf site to form the dehydrated products shown in Scheme 1.

The resulting rate law, assuming EP* as the most abundant reactive intermediate (MARI) and step 3 as the rate-determining step, is shown in eq 2 (see Section S3 for the full derivation).

$$\frac{r_{aldol}}{[L]} = \frac{\gamma_{EP*}}{\gamma_{\ddagger}} k_3 K_2 K_1 a_{EP} \qquad (2)$$

where r_{aldol} is the total rate of all aldol condensation products (hydrated or dehydrated), $[L]$ is the number of closed Hf sites, γ_{EP*} is the activity coefficient of Hf-adsorbed EP, $\gamma_{\ddagger}$ is the activity coefficient of the transition state, and k_3, K_2, and K_1 are the rate and equilibrium constants corresponding to the relevant steps shown in Scheme 2. The activity coefficients and constants k_3, K_2, and K_1 cannot be deconvoluted experimentally and thus are lumped into a single apparent rate constant, k_{app}, giving a rate expression (eq 3) that can be fitted to the data for interpretation

$$\frac{r_{aldol}}{[L]} = k_{app} a_{EP} \qquad (3)$$

To confirm this form of the rate expression, for a given temperature curve, the data can be fit to a power law with the form $y = ba_{EP}^{\gamma}$ to determine the order of reaction with respect to EP. Values of y in both solvents and framework polarities across the range of temperatures are between 0.8 and 1.3 (Table S1), indicating predominantly first-order kinetics with respect to EP under the studied activity ranges. The observed first-order kinetics for aldol addition systems are consistent with previous gas-phase studies of aldol condensation/esterification in Ti-BEA zeolites, indicating that the nucleophilic attack on the second adsorbed carbonyl by the enolate is rate-determining,[38] with the additional assumption of the most-abundant reactive intermediate as EP*. Several other studies over catalysts have shown enolate formation (step 1) to be rate-determining;[42,58] however, kinetically relevant enolate formation would only yield a first-order rate law in our system if the MARI is assumed to be a vacant Hf site (see Section S3 for derivations), which is unlikely during liquid-phase catalysis where active sites are expected to be saturated with either strongly binding oxygenates such as EP or a coordinating solvent.

Apparent first-order rate constants as functions of inverse temperature are shown in Figure 3. Rate constants vary by
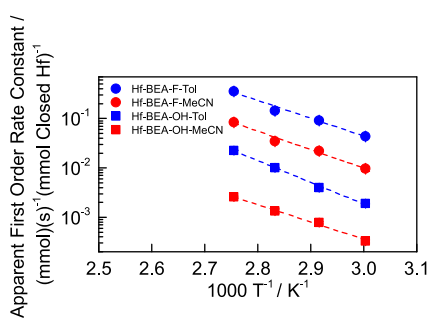

Figure 3. Apparent first-order rate constants for EP aldol addition (k_{app}, normalized per closed Hf) regressed from data in Figure 2 measured on Hf-BEA-F(327) and Hf-BEA-OH(145) in toluene and acetonitrile as functions of inverse temperature. Dashed lines are exponential fits to the data.

frameworks. Apparent first-order rate constants can be expressed in terms of enthalpic and entropic contributions according to eq 4.

$$k_{app} = \frac{k_B T}{h} e^{-\Delta G_{app}/RT} = \frac{k_B T}{h} e^{-\Delta H_{app}/RT} e^{\Delta S_{app}/R} \qquad (4)$$

where k_B is Boltzmann's constant, T is the reaction temperature, h is Planck's constant, and R is the ideal gas constant. ΔH_{app} and ΔS_{app} are the apparent enthalpic and entropic barriers, respectively, for the aldol addition reaction and represent the combined kinetics of enolate formation (step 1 in Scheme 2), adsorption of a second EP molecule to the Hf active site (step 2), and carbon–carbon bond formation (step 3). These apparent kinetic parameters also include excess contributions due to potential deviations from an ideal MARI and transition state ($\gamma_{EP*}/\gamma_{\ddagger}$ in eq 2). Enthalpies and entropies are calculated via the linearization of eq 4 and subsequent transformation of the typical Arrhenius $1/T$ x-axis to be relative to the harmonic mean temperature of the system, such that the new x-axis is $(1/T - 1/T_{hm})$ (details of this transformation are in Section S3).[47] The resulting transformation allows for the calculation of ΔH_{app} from the slope and ΔG_{app} from the intercept of the transformed Arrhenius plot, from which ΔS_{app} can be calculated.

Table 2 shows ΔH_{app} and ΔS_{app} values for the four systems. Despite aldol addition rates varying by several orders of

Table 2. ΔH_{app} and ΔS_{app} Values for EP Aldol Addition in Hf-BEA-F(327) and Hf-BEA-OH(145) in Toluene and Acetonitrile, Extracted from Apparent First-Order Rate Constants

catalyst	solvent	ΔH_{app}/kJ mol^{-1}	ΔS_{app}/J mol^{-1}K^{-1}
Hf-BEA-F	toluene	67.9 ± 6	−68.5 ± 19
	acetonitrile	70.2 ± 6	−74.0 ± 18
Hf-BEA-OH	toluene	83.8 ± 4	−47.0 ± 10
	acetonitrile	67.7 ± 4	−109 ± 11

magnitude between the four systems; apparent enthalpies are ~70 kJ mol^{-1}, with the exception of Hf-BEA-OH-Tol, which has an enthalpic barrier approximately 15 kJ mol^{-1} higher than the other three systems. Entropic barriers in both solvents for Hf-BEA-F are similar around ~70 J mol^{-1} K^{-1}, while the entropic barrier is higher (more positive) in Hf-BEA-OH-Tol (−47 J mol^{-1} K^{-1}) and lower (more negative) in Hf-BEA-OH-MeCN (−109 J mol^{-1} K^{-1}). Taken together, these results allow us to draw several conclusions about the nature of aldol addition reactions in these systems.

Based on eq 2, the apparent free energy barrier (and the component enthalpic and entropic barriers) represents the sum of the barriers for enolate formation, second EP adsorption, and nucleophilic attack, as well as the difference in excess free energy between the MARI and the transition state (ΔG_{EP*}^{E} and $\Delta G_{\ddagger}^{E}$ respectively). Differences in apparent reaction enthalpies and entropies between two systems can be rationalized as changes in the apparent Gibbs free energy ($\Delta\Delta G_{app}$), reflecting differing stabilities of the transition state, MARI, or solution-phase EP between solvents and frameworks, shown in eq 5 (derivation in Section S3)

$$\Delta\Delta G_{app} = (\Delta G_{\ddagger} - \Delta G_{\ddagger}^{E}) - (\Delta G_{EP*} - \Delta G_{EP*}^{E}) - \Delta G_{EP} \qquad (5)$$

~100× across the four catalyst/solvent systems, as expected from the differences in observed rates in Figure 2. For a given solvent, rate constants at 363 K are 1 order of magnitude higher in Hf-BEA-F than Hf-BEA-OH.

Interpretation of data in Figure 3 using transition state theory can give further insights into the effect of different

where $\Delta G_{\ddagger}$, ΔG_{EP*}, and ΔG_{EP} are the differences in Gibbs free energy of the transition state, adsorbed EP, and solution-phase EP between two systems. If toluene and acetonitrile interacted with adsorbed species significantly differently, G_{EP*}^{E} and $G_{\ddagger}^{E}$ would take on different values in each solvent, manifesting in different enthalpic and entropic barriers for Hf-BEA-F-Tol and Hf-BEA-F-MeCN. Since enthalpic and entropic barriers are within the error of each other for both solvents in Hf-BEA-F, we posit that either the difference in excess free energies for adsorbed species is similar for toluene and acetonitrile or that for a given solvent, $\Delta G_{\ddagger}^{E}$ and ΔG_{EP*}^{E} are approximately equal and cancel in eq 5.

Additionally, deprotonation of adsorbed EP to form an enolate (step 1) and nucleophilic attack (step 3) are relatively short-range interactions between atoms that are immediately adjacent and unlikely to be affected by solvent molecules or silanol defects that may be several atomic lengths away from the active site. In contrast, step 2 requires the adsorption of a second EP molecule from the bulk of the pore onto the active site, which might require the displacement of adjacent solvents or EP molecules and formation or breaking of bonds with silanol nests. Thus, we hypothesize that modifications to the pore hydrophobicity and solvents would most likely affect the adsorption of a second EP molecule to the active site in step 2.

Apparent enthalpies and entropies of EP aldol addition in both solvents are strikingly similar for Hf-BEA-F despite the very different polarity of toluene and acetonitrile (dielectric constants of 2.3 and 35.9, respectively[59]). The reported entropies are most likely representative of the entropy loss upon formation of the C−C bond during a nucleophilic attack. The similar apparent entropies also imply that EP is not tightly solvated by a shell of acetonitrile molecules that must be broken apart during EP adsorption to the active site. Stronger solvation shells have been observed for alcohol solvents that can form strong hydrogen-bonding networks, whose disruptions carry an enthalpic penalty and yield a release of entropy.[45,47] Despite the absence of a solvent effect on apparent enthalpies and a minimal effect on apparent entropies, apparent first-order rate constants in acetonitrile are still consistently 4× lower than in toluene, suggesting that lower rates arise from acetonitrile coordinating to and poisoning acid sites.[60,61] This implies that a certain fraction of active sites is consistently covered by acetonitrile, with the remainder being covered predominantly by the EP* MARI, yielding similar kinetics to Hf-BEA-F-Tol but with fewer available active sites.

In contrast to Hf-BEA-F, there is an observed solvent effect in Hf-BEA-OH. Thus, the differences in kinetics between Hf-BEA-OH-Tol and Hf-BEA-OH-MeCN must be due to the interactions between EP, the solvent, and silanol nests. The apparent reaction enthalpy in Hf-BEA-OH-Tol is ∼15 kJ mol^{-1} higher than the enthalpies in Hf-BEA-F. Given that silanol nests are many atomic lengths away from the active site, the presence of silanol nests is unlikely to alter enolate formation (step 1) or nucleophilic attack (step 3). Thus, differences in kinetics are likely to involve silanol nests affecting EP adsorption (step 2). Silanol groups are expected to form hydrogen bonds with carbonyl groups on EP molecules that must be broken before EP can adsorb to the active site for reaction, which would account for the increased apparent enthalpic barrier in the hydrophilic framework. The apparent entropy is also ∼20 J mol^{-1} K^{-1} more positive in Hf-BEA-OH-Tol than in Hf-BEA-F-Tol, indicating that the liberation of an

EP from a silanol nest to react on a Hf site results in a slight entropy gain, although the formation of a C−C bond during the rate-determining step still leads to an entropy that is overall negative.

EP Absorption into Si-BEA Frameworks. To further understand the pore environment in the four systems, liquid-phase EP absorption isotherms were measured in hydrophobic Si-BEA-F and hydrophilic Si-BEA-OH across a similar range of EP activities as in Figure 2. The goal of these experiments was to determine the extent to which EP, toluene, or acetonitrile fill BEA pores in analogous polarity environments but in the absence of framework Lewis acid sites. Specifically, if EP uptake was both similar and consistently high in different solvents and frameworks across EP activities, it would imply that similarities in the kinetics could be ascribed to an EP-filled pore with a negligible solvent to influence reaction kinetics.

EP uptake per gram of Si-BEA-F and Si-BEA-OH (dealuminated BEA) in the two solvents is shown in Figure 4. EP
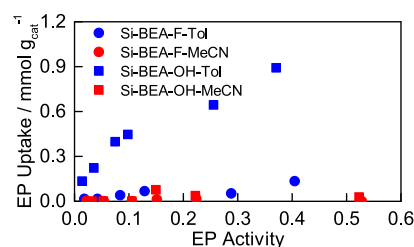

Figure 4. EP uptake (mmol g$_{cat}^{-1}$) as a function of EP activity in Si-BEA-F and Si-BEA-OH frameworks in both toluene and acetonitrile. Measurements were taken after 24 h of equilibration time at 298 K.

absorption into the frameworks in toluene generally increased with increasing EP activity, with EP uptake being 5−10× higher in Si-BEA-OH-Tol than Si-BEA-F-Tol. In contrast, EP uptake was lower or negligible at all activities studied in acetonitrile for a given framework. Thus, appreciable amounts of EP likely accumulate in the zeolite pores when the reaction is performed in toluene (Scheme 3a,c); however, pores are likely predominantly filled with the solvent when reactions are performed in acetonitrile (Scheme 3b,d). The result of the different concentrations of EP in the pore, however, exhibits nearly identical reaction enthalpies for Hf-BEA-F-Tol and Hf-BEA-F-MeCN (Table 2), where rate constants in the two systems generally differ by a constant at a given temperature. This implies that while the pore volumes are largely filled with acetonitrile in Hf-BEA-F-MeCN, some fraction of the Hf sites is still covered by the MARI (EP*) during catalysis. We thus conclude that in Hf-BEA-F, the polarity of the solvent minimally affects EP adsorption onto the active site. While polar acetonitrile might be expected to solvate EP more tightly than nonpolar toluene, any solvation shell around EP must be relatively weakly coordinated. These absorption data also provide evidence against the possibility that kinetics are nearly solvent-agnostic in Hf-BEA-F due to clustering of excess EP near the active site or within the pores regardless of the bulk solvent, given that EP uptake is so low in acetonitrile. However, due to the inherent differences between equilibrium liquid-phase absorption measurements and actual reaction conditions, the possibility of EP clustering near the active site cannot be entirely ruled out.

Hf-BEA-OH-MeCN has the same apparent enthalpic barrier as both Hf-BEA-F systems (Table 2), implying that the silanol

Scheme 3. Depictions of Pore Environments in (a) Hf-BEA-F-Tol, (b) Hf-BEA-F-MeCN, (c) Hf-BEA-OH-Tol, and (d) Hf-BEA-OH-MeCN Based on Kinetic and EP Absorption Data[a]

(a) **Hf-BEA-F-Tol**　　(b) **Hf-BEA-F-MeCN**

(c) **Hf-BEA-OH-Tol**　　(d) **Hf-BEA-OH-MeCN**
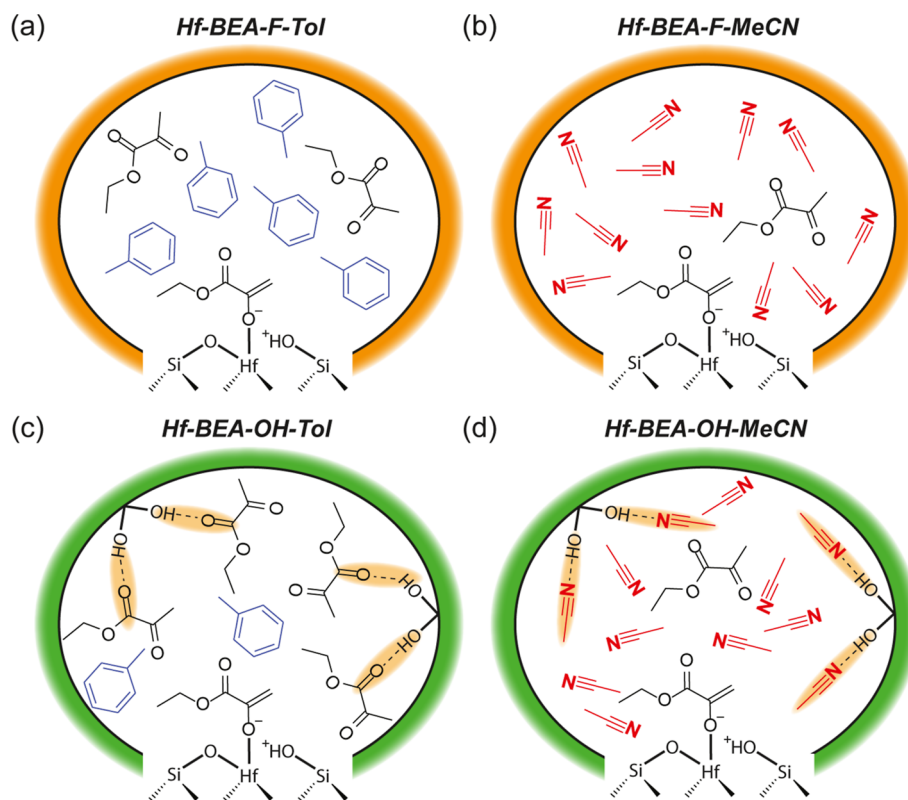
[a]Numbers of molecules depicted in each figure are not rigorously quantitative and are intended to qualitatively reflect different levels of EP uptake in the four systems from absorption data in Figure 4.

nests in this catalyst do not influence aldol addition kinetics. Based on the data in Figure 4, the pores of Hf-BEA-OH-MeCN are predominantly filled with acetonitrile, implying that silanol nests are blocked by acetonitrile and unable to coordinate with EP (Scheme 3d). Hf-BEA-OH-Tol has an apparent enthalpic barrier ~15 kJ mol^{-1} higher than the other systems studied and is also the only system that is likely to have hydrogen bonds present between the framework and intraporous EP (Scheme 3c). Thus, these hydrogen bonds inhibit EP adsorption to Hf active sites much more significantly than interactions between EP and a solvent.

Solvents have been shown to affect rates via increased enthalpic penalties to substrate adsorption in zeolites for other chemistries; however, many of these differences can be attributed to the presence of strong hydrogen-bonding networks. Tan et al. reported rate constants for 1-octene epoxidation over Ti-BEA-OH that were enhanced by a factor of 20× (normalized per Ti) when performed in acetonitrile instead of methanol.[62] Lower rates in methanol were attributed predominantly to changes in the Gibbs free energy of adsorption of 1-octene, which results in the displacement of multiple solvent molecules. The rupture of hydrogen bonds is more severe in methanol than in acetonitrile, resulting in a greater enthalpic cost toward the adsorption step. These effects were more pronounced on larger alkenes.[63] The rupture of hydrogen bond networks was also responsible for a 70 J mol^{-1} K^{-1} higher entropic release upon cyclohexanone adsorption in Sn-BEA-F than Sn-BEA-OH during MPVO catalysis in a 2-butanol solvent. Our results stand in contrast to the aforementioned studies; aldol addition kinetics in hydrophobic

Lewis acidic zeolites are agnostic to the solvent in hydrophobic frameworks beyond site-blocking effects of coordinating solvents. It is important to note that the solvents tested in this study do not form extensive hydrogen-bonding networks, which may also be responsible for the minimal differences in reaction kinetics between toluene and acetonitrile. The only system studied here in which hydrogen bonding may be present is Hf-BEA-OH-Tol, where EP molecules may be bound to silanol nests. Accordingly, this is also the only system with a distinctly higher apparent enthalpy of reaction.

Effect of Water on Aldol Addition Rates. While water is known to possess a strong inhibition rate over many Lewis acid catalysts, Lewis acidic zeolites are known to tolerate appreciable quantities of water.[64−66] The disruption of confined water clusters near silanol nests has even been shown to lead to higher 1-octene epoxidation turnover rates in Ti-BEA-OH as compared to Ti-BEA-F.[45] To determine the effect of water on EP aldol addition rates in Hf-BEA-F and Hf-BEA-OH, the water concentration was varied in acetonitrile (0.02 M < C_{water} < 2 M, 0.0005 < a_{water} < 0.05 at constant C_{EP} = 0.1 M). Due to the immiscibility of toluene and water, rates of aldol addition in the presence of water were only studied in acetonitrile. Figure 5 shows that the rates of aldol addition in Hf-BEA-F-MeCN and Hf-BEA-OH-MeCN decrease by approximately 3× and 7×, respectively, as the activity of water is increased by 2 orders of magnitude. Fitting these rates to a power law with respect to water ($r_{aldol} = ba_{H_2O}^y$) yields y = −0.2 for Hf-BEA-F-MeCN and −0.4 for Hf-BEA-OH-MeCN, indicating a relatively weak inhibitory effect of water on the
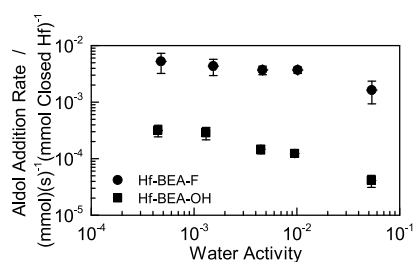
Figure 5. EP aldol addition rates (per closed Hf) as a function of water activity (0.02−2 M H_2O) at 363 K and C_{EP} = 0.1 M in acetonitrile in Hf-BEA-F and Hf-BEA-OH.

reaction in the liquid phase for both systems. As can be expected, Hf-BEA-OH has a stronger interaction with water than Hf-BEA-F, likely due to water's preferential absorption into hydrophilic pores, facilitating poisoning of Hf sites. This inhibitory effect is slightly more pronounced than previously observed effects of water addition on gas-phase acetaldehyde aldol addition rates over Ti-BEA zeolites,[38] but the relatively weak dependence of rate on water activity showcases the overall high water tolerance of these catalysts at lower conversion. For an aldol condensation reaction at high conversion where stoichiometric amounts of water are generated, water removal may be required to avoid excessive catalyst activity loss.

CONCLUSIONS

We have studied the effect of framework polarity and solvent on the aldol addition kinetics of EP in Hf-BEA zeolites. EP aldol addition rates were predominantly catalyzed on closed Hf sites and were uniformly first-order in all four solvent/catalyst systems studied, consistent with the nucleophilic attack of a second adsorbed EP by the enolate as the rate-determining step with adsorbed EP as the MARI. First-order rate constants spanned 2 orders of magnitude in the order of Hf-BEA-F-Tol > Hf-BEA-F-MeCN > Hf-BEA-OH-Tol > Hf-BEA-OH-MeCN. Apparent enthalpic and entropic barriers in hydrophobic Hf-BEA-F are within the experimental error of each other for both toluene and acetonitrile, despite rate constants that are 4× lower in acetonitrile. A solvent effect was observed in hydrophilic Hf-BEA-OH, where enthalpies were ~15 kJ mol^{-1} higher in Hf-BEA-OH-Tol than in the other three systems.

EP absorption isotherms in Si-BEA-F and Si-BEA-OH show that EP uptake in both hydrophobic and hydrophilic frameworks is nearly negligible in acetonitrile but increases with EP activity in toluene. This indicates that the pore is saturated with the solvent when performed in acetonitrile but contains a mixture of the solvent and EP when performed in toluene. Taken alongside the kinetic data, we can conclude that polar solvents minimally affect substrate adsorption kinetics in Hf-BEA-F pores. Silanol nests can inhibit substrate adsorption via hydrogen bonding in Hf-BEA-OH, but this effect is inhibited by the presence of acetonitrile, which can itself coordinate to the silanol nests and block EP-silanol interactions. In both catalysts, polar solvents reduce aldol addition rate constants largely through active site poisoning, which is more pronounced in hydrophilic frameworks. Water was observed to have a relatively minor effect on aldol addition rates except at concentrations approaching 2 M, with a 3× and 7× decrease in rate across 2 orders of magnitude of water activity for Hf-BEA-F and Hf-BEA-OH, respectively.

Taken collectively, these results indicate that the choice of solvent and framework polarity of Hf-BEA significantly affect aldol rates, but adsorption kinetics are only affected when the substrate is able to undergo hydrogen bonding with silanol nests. This has significant implications for the choice of solvent and catalyst when running liquid-phase aldol condensation reactions in microporous media and can be extended toward optimizing other aldol condensation rates and selectivities for biomass-derived compounds.

■ ASSOCIATED CONTENT

Ⓢ Supporting Information

The Supporting Information is available free of charge at https://pubs.acs.org/doi/10.1021/acscatal.3c00787.

> Catalyst characterization (XRD, FTIR, and UV−vis); reaction kinetics control (GC chromatograms, GC−MS spectra of products, kinetic controls, product distributions, and power law fits); and rate law derivations and kinetic analysis (aldol addition rate equation derivation, and harmonic mean-temperature transformation) (PDF)

■ AUTHOR INFORMATION

Corresponding Author

Yuriy Román-Leshkov − *Department of Chemical Engineering, Massachusetts Institute of Technology, Cambridge, Massachusetts 02139, United States;* ⓘ orcid.org/0000-0002-0025-4233; Email: yroman@mit.edu

Authors

Alexander A. Khechfe − *Department of Chemical Engineering, Massachusetts Institute of Technology, Cambridge, Massachusetts 02139, United States;* ⓘ orcid.org/0000-0002-1849-3582

Thaïs B. M. Matha − *Department of Chemical Engineering, Massachusetts Institute of Technology, Cambridge, Massachusetts 02139, United States;* ⓘ orcid.org/0000-0002-4815-3415

Complete contact information is available at:
https://pubs.acs.org/10.1021/acscatal.3c00787

Notes

The authors declare no competing financial interest.

are those of the author(s) and do not necessarily reflect the views of the National Science Foundation.

■ REFERENCES

(1) Palagin, D.; Sushkevich, V. L.; Ivanova, I. I. C−C Coupling Catalyzed by Zeolites: Is Enolization the Only Possible Pathway for Aldol Condensation? *J. Phys. Chem. C* **2016**, *120*, 23566−23575.

(2) Manzer, L. E. Catalytic synthesis of α-methylene-γ-valerolactone: a biomass-derived acrylic monomer. *Appl. Catal., A* **2004**, *272*, 249−256.

(3) Chheda, J. N.; Dumesic, J. A. An Overview of Dehydration, Aldol-Condensation and Hydrogenation Processes for Production of Liquid Alkanes from Biomass-Derived Carbohydrates. *Catal. Today* **2007**, *123*, 59−70.

(4) Barrett, C. J.; Chheda, J. N.; Huber, G. W.; Dumesic, J. A. Single-Reactor Process for Sequential Aldol-Condensation and Hydrogenation of Biomass-Derived Compounds in Water. *Appl. Catal., B* **2006**, *66*, 111−118.

(5) Chang, H.; Gilcher, E. B.; Huber, G. W.; Dumesic, J. A. Synthesis of Performance-Advantaged Polyurethanes and Polyesters from Biomass-Derived Monomers by Aldol-Condensation of 5-Hydroxymethyl Furfural and Hydrogenation. *Green Chem.* **2021**, *23*, 4355−4364.

(6) West, R. M.; Liu, Z. Y.; Peter, M.; Gärtner, C. A.; Dumesic, J. A. Carbon−Carbon Bond Formation for Biomass-Derived Furfurals and Ketones by Aldol Condensation in a Biphasic System. *J. Mol. Catal. A: Chem.* **2008**, *296*, 18−27.

(7) Vollhardt, K. P. C.; Shore, N. E. *Organic Chemistry: Structure and Function*, 7th ed.; Macmillan Learning, 2014; pp 800−806.

(8) Gathergood, N.; Juhl, K.; Poulsen, T. B.; Thordrup, K.; Jørgensen, K. A. Direct Catalytic Asymmetric Aldol Reactions of Pyruvates: Scope and Mechanism. *Org. Biomol. Chem.* **2004**, *2*, 1077−1085.

(9) Al-Naji, M.; Puértolas, B.; Kumru, B.; Cruz, D.; Bäumel, M.; Schmidt, B. V. K. J.; Tarakina, N. V.; Pérez-Ramírez, J. Sustainable Continuous Flow Valorization of γ-Valerolactone with Trioxane to α-Methylene-γ-Valerolactone over Basic Beta Zeolites. *ChemSusChem* **2019**, *12*, 2628−2636.

(10) Zhang, G.; Hattori, H.; Tanabe, K. Aldol Addition of Acetone, Catalyzed by Solid Base Catalysts: Magnesium Oxide, Calcium Oxide, Strontium Oxide, Barium Oxide, Lanthanum (III) Oxide and Zirconium Oxide. *Appl. Catal.* **1988**, *36*, 189−197.

(11) Di Cosimo, J. I.; Díez, V. K.; Apesteguía, C. R. Base catalysis for the synthesis of α,β-unsaturated ketones from the vapor-phase aldol condensation of acetone. *Appl. Catal., A* **1996**, *137*, 149−166.

(12) Machajewski, T. D.; Wong, C.-H. The Catalytic Asymmetric Aldol Reaction. *Angew. Chem., Int. Ed.* **2000**, *39*, 1352−1375.

(13) Kumagai, N.; Shibasaki, M. Recent Advances in Direct Catalytic Asymmetric Transformations under Proton-Transfer Conditions. *Angew. Chem., Int. Ed.* **2011**, *50*, 4760−4772.

(14) Corma, A.; Nemeth, L. T.; Renz, M.; Valencia, S. Sn-Zeolite Beta as a Heterogeneous Chemoselective Catalyst for Baeyer-Villiger Oxidations. *Nature* **2001**, *412*, 423−425.

(15) Moliner, M. State of the Art of Lewis Acid-Containing Zeolites: Lessons from Fine Chemistry to New Biomass Transformation Processes. *Dalton Trans.* **2014**, *43*, 4197−4208.

(16) Nikolla, E.; Román-Leshkov, Y.; Moliner, M.; Davis, M. E. One-Pot" Synthesis of 5-(Hydroxymethyl)Furfural from Carbohydrates Using Tin-Beta Zeolite. *ACS Catal.* **2011**, *1*, 408−410.

(17) Rodríguez-Fernández, A.; Di Iorio, J. R.; Paris, C.; Boronat, M.; Corma, A.; Román-Leshkov, Y.; Moliner, M. Selective Active Site Placement in Lewis Acid Zeolites and Implications for Catalysis of Oxygenated Compounds. *Chem. Sci.* **2020**, *11*, 10225−10235.

(18) Corma, A.; Domine, M. E.; Valencia, S. Water-Resistant Solid Lewis Acid Catalysts: Meerwein−Ponndorf−Verley and Oppenauer Reactions Catalyzed by Tin-Beta Zeolite. *J. Catal.* **2003**, *215*, 294−304.

(19) Corma, A.; Renz, M. Sn-Beta Zeolite as Diastereoselective Water-Resistant Heterogeneous Lewis-Acid Catalyst for Carbon−Carbon Bond Formation in the Intramolecular Carbonyl − Ene Reaction. *Chem. Commun.* **2004**, *0*, 550−551.

(20) Dijkmans, J.; Dusselier, M.; Gabriëls, D.; Houthoofd, K.; Magusin, P. C. M. M.; Huang, S.; Pontikes, Y.; Trekels, M.; Vantomme, A.; Giebeler, L.; et al. Cooperative Catalysis for Multistep Biomass Conversion with Sn/Al Beta Zeolite. *ACS Catal.* **2015**, *5*, 928−940.

(21) Ennaert, T.; Van Aelst, J.; Dijkmans, J.; De Clercq, R.; Schutyser, W.; Dusselier, M.; Verboekend, D.; Sels, B. F. Potential and Challenges of Zeolite Chemistry in the Catalytic Conversion of Biomass. *Chem. Soc. Rev.* **2016**, *45*, 584−611.

(22) Ferrini, P.; Dijkmans, J.; De Clercq, R.; Van de Vyver, S.; Dusselier, M.; Jacobs, P. A.; Sels, B. F. Lewis Acid Catalysis on Single Site Sn Centers Incorporated into Silica Hosts. *Coord. Chem. Rev.* **2017**, *343*, 220−255.

(23) Hernández, B.; Iglesias, J.; Morales, G.; Paniagua, M.; López-Aguado, C.; García Fierro, J. L.; Wolf, P.; Hermans, I.; Melero, J. A. One-Pot Cascade Transformation of Xylose into γ-Valerolactone (GVL) over Bifunctional Brønsted−Lewis Zr−Al-Beta Zeolite. *Green Chem.* **2016**, *18*, 5777−5781.

(24) Gounder, R.; Iglesia, E. Catalytic Consequences of Spatial Constraints and Acid Site Location for Monomolecular Alkane Activation on Zeolites. *J. Am. Chem. Soc.* **2009**, *131*, 1958−1971.

(25) Auerbach, S. M.; Carrado, K. A.; Dutta, P. K. *Handbook of Zeolite Science and Technology*; CRC press, 2003.

(26) Olsbye, U.; Svelle, S.; Bjørgen, M.; Beato, P.; Janssens, T. V. W.; Joensen, F.; Bordiga, S.; Lillerud, K. P. Conversion of Methanol to Hydrocarbons: How Zeolite Cavity and Pore Size Controls Product Selectivity. *Angew. Chem., Int. Ed.* **2012**, *51*, 5810−5831.

(27) Jentys, A.; Warecka, G.; Derewinski, M.; Lercher, J. A. Adsorption of Water on ZSM5 Zeolites. *J. Phys. Chem.* **1989**, *93*, 4837−4843.

(28) Gounder, R.; Davis, M. E. Beyond Shape Selective Catalysis with Zeolites: Hydrophobic Void Spaces in Zeolites Enable Catalysis in Liquid Water. *AIChE J.* **2013**, *59*, 3349−3358.

(29) Bates, J. S.; Gounder, R. Influence of Confining Environment Polarity on Ethanol Dehydration Catalysis by Lewis Acid Zeolites. *J. Catal.* **2018**, *365*, 213−226.

(30) Corma, A.; Llabrés I Xamena, F. X.; Prestipino, C.; Renz, M.; Valencia, S. Water Resistant, Catalytically Active Nb and Ta Isolated Lewis Acid Sites, Homogeneously Distributed by Direct Synthesis in a Beta Zeolite. *J. Phys. Chem. C* **2009**, *113*, 11306−11315.

(31) Luo, H. Y.; Lewis, J. D.; Román-Leshkov, Y. Lewis Acid Zeolites for Biomass Conversion: Perspectives and Challenges on Reactivity, Synthesis, and Stability. *Annu. Rev. Chem. Biomol. Eng.* **2016**, *7*, 663−692.

(32) Bui, L.; Luo, H.; Gunther, W. R.; Román-Leshkov, Y. Domino Reaction Catalyzed by Zeolites with Brønsted and Lewis Acid Sites for the Production of γ-Valerolactone from Furfural. *Angew. Chem., Int. Ed.* **2013**, *52*, 8022−8025.

(33) Li, C.; Ferri, P.; Paris, C.; Moliner, M.; Boronat, M.; Corma, A. Design and Synthesis of the Active Site Environment in Zeolite Catalysts for Selectively Manipulating Mechanistic Pathways. *J. Am. Chem. Soc.* **2021**, *143*, 10718−10726.

(34) Lewis, J. D.; Ha, M.; Luo, H.; Faucher, A.; Michaelis, V. K.; Románromán-Leshkov, Y. Distinguishing Active Site Identity in Sn-Beta Zeolites Using 31 P MAS NMR of Adsorbed Trimethylphosphine Oxide. *ACS Catal.* **2018**, *8*, 3076.

(35) Van de Vyver, S.; Román-Leshkov, Y. Metalloenzyme-Like Zeolites as Lewis Acid Catalysts for C-C Bond Formation. *Angew. Chem., Int. Ed.* **2015**, *54*, 12554−12561.

(36) Kikhtyanin, O.; Kelbichová, V.; Vitvarová, D.; Kubů, M.; Kubička, D. Aldol Condensation of Furfural and Acetone on Zeolites. *Catal. Today* **2014**, *227*, 154−162.

(37) Wang, Y.; Lewis, J. D.; Román-Leshkov, Y. Synthesis of Itaconic Acid Ester Analogues via Self-Aldol Condensation of Ethyl Pyruvate Catalyzed by Hafnium BEA Zeolites. *ACS Catal.* **2016**, *6*, 2739−2744.

(38) Zhang, Z.; Berdugo-Díaz, C. E.; Bregante, D. T.; Zhang, H.; Flaherty, D. W. Aldol Condensation and Esterification over Ti-

Substituted *BEA Zeolite: Mechanisms and Effects of Pore Hydrophobicity. *ACS Catal.* **2022**, *12*, 1481−1496.

(39) Lewis, J. D.; Van de Vyver, S.; Román Leshkov, Y. Acid−Base Pairs in Lewis Acidic Zeolites Promote Direct Aldol Reactions by Soft Enolization. *Angew. Chem.* **2015**, *127*, 9973−9976.

(40) Yang, G.; Zhou, L.; Han, X. Lewis and Brönsted Acidic Sites in M4+-Doped Zeolites (M = Ti, Zr, Ge, Sn, Pb) as Well as Interactions with Probe Molecules: A DFT Study. *J. Mol. Catal. A: Chem.* **2012**, *363−364*, 371−379.

(41) Van de Vyver, S.; Odermatt, C.; Romero, K.; Prasomsri, T.; Román-Leshkov, Y. Solid Lewis Acids Catalyze the Carbon−Carbon Coupling between Carbohydrates and Formaldehyde. *ACS Catal.* **2015**, *5*, 972−977.

(42) Wang, S.; Iglesia, E. Substituent Effects and Molecular Descriptors of Reactivity in Condensation and Esterification Reactions of Oxygenates on Acid-Base Pairs at TiO2 and ZrO2 Surfaces. *J. Phys. Chem. C* **2016**, *120*, 21589−21616.

(43) Zhang, H.; Ibrahim, M. Y. S.; Flaherty, D. W. Aldol Condensation among Acetaldehyde and Ethanol Reactants on TiO2: Experimental Evidence for the Kinetically Relevant Nucleophilic Attack of Enolates. *J. Catal.* **2018**, *361*, 290−302.

(44) Kadam, S. A.; Hwang, A.; Iglesia, E. Consequences of Intrapore Liquids on Reactivity, Selectivity, and Stability for Aldol Condensation Reactions on Anatase TiO2 Catalysts. *ChemCatChem* **2022**, *14*, No. e202200059.

(45) Bregante, D. T.; Johnson, A. M.; Patel, A. Y.; Ayla, E. Z.; Cordon, M. J.; Bukowski, B. C.; Greeley, J.; Gounder, R.; Flaherty, D. W. Cooperative Effects between Hydrophilic Pores and Solvents: Catalytic Consequences of Hydrogen Bonding on Alkene Epoxidation in Zeolites. *J. Am. Chem. Soc.* **2019**, *141*, 7302−7319.

(46) Cordon, M.; Harris, J. W.; Vega-Vila, J. C.; Bates, J. S.; Kaur, S.; Gupta, M.; Witzke, M. E.; Wegener, E. C.; Miller, J. T.; Flaherty, D. W.; et al. Dominant Role of Entropy in Stabilizing Sugar Isomerization Transition States within Hydrophobic Zeolite Pores. *J. Am. Chem. Soc.* **2018**, *140*, 14244−14266.

(47) Di Iorio, J. R.; Johnson, B. A.; Román-Leshkov, Y. Ordered Hydrogen-Bonded Alcohol Networks Confined in Lewis Acid Zeolites Accelerate Transfer Hydrogenation Turnover Rates. *J. Am. Chem. Soc.* **2020**, *142*, 19379−19392.

(48) Johnson, B. A.; Di Iorio, J. R.; Román-Leshkov, Y. Identification and quantification of distinct active sites in Hf-Beta zeolites for transfer hydrogenation catalysis. *J. Catal.* **2021**, *404*, 607.

(49) Baran, R.; Millot, Y.; Onfroy, T.; Krafft, J. M.; Dzwigaj, S. Influence of the Nitric Acid Treatment on Al Removal, Framework Composition and Acidity of BEA Zeolite Investigated by XRD, FTIR and NMR. *Microporous Mesoporous Mater.* **2012**, *163*, 122−130.

(50) Eckstein, S.; Hintermeier, P. H.; Zhao, R.; Baráth, E.; Shi, H.; Liu, Y.; Lercher, J. A. Influence of Hydronium Ions in Zeolites on Sorption. *Angew. Chem., Int. Ed.* **2019**, *58*, 3450−3455.

(51) Peeters, E.; Calderon-Ardila, S.; Hermans, I.; Dusselier, M.; Sels, B. F. Toward Industrially Relevant Sn-BETA Zeolites: Synthesis, Activity, Stability, and Regeneration. *ACS Catal.* **2022**, *12*, 9559−9569.

(52) Harris, J. W.; Cordon, M. J.; Di Iorio, J. R.; Vega-Vila, J. C.; Ribeiro, F. H.; Gounder, R. Titration and Quantification of Open and Closed Lewis Acid Sites in Sn-Beta Zeolites That Catalyze Glucose Isomerization. *J. Catal.* **2016**, *335*, 141−154.

(53) Roy, S.; Bakhmutsky, K.; Mahmoud, E.; Lobo, R. F.; Gorte, R. J. Probing Lewis Acid Sites in Sn-Beta Zeolite. *ACS Catal.* **2013**, *3*, 573−580.

(54) Johnson, B. A.; Di Iorio, J. R.; Román-Leshkov, Y. Tailoring Distinct Reactive Environments in Lewis Acid Zeolites for Liquid Phase Catalysis. *Acc. Mater. Res.* **2021**, *2*, 1033−1046.

(55) Rojas-Buzo, S.; Concepción, P.; Corma, A.; Moliner, M.; Boronat, M. In-Situ-Generated Active Hf-Hydride in Zeolites for the Tandem N-Alkylation of Amines with Benzyl Alcohol. *ACS Catal.* **2021**, *11*, 8049−8061.

(56) Madon, R. J.; Iglesia, E. Catalytic Reaction Rates in Thermodynamically Non-Ideal Systems. *J. Mol. Catal. A: Chem.* **2000**, *163*, 189−204.

(57) Madon, R. J.; Boudart, M. Experimental Criterion for the Absence of Artifacts in the Measurement of Rates of Heterogeneous Catalytic Reactions. *Ind. Eng. Chem. Fundam.* **2002**, *21*, 438−447.

(58) Wang, S.; Iglesia, E. Entropy-Driven High Reactivity of Formaldehyde in Nucleophilic Attack by Enolates on Oxide Surfaces. *J. Am. Chem. Soc.* **2018**, *140*, 775−782.

(59) Ritzoulis, G.; Papadopoulos, N.; Jannakoudakis, D. Densities, viscosities, and dielectric constants of acetonitrile + toluene at 15, 25, and 35 .degree.C. *J. Chem. Eng. Data* **1986**, *31*, 146−148.

(60) Tang, B.; Dai, W.; Wu, G.; Guan, N.; Li, L.; Hunger, M. Improved Postsynthesis Strategy to Sn-Beta Zeolites as Lewis Acid Catalysts for the Ring-Opening Hydration of Epoxides. *ACS Catal.* **2014**, *4*, 2801−2810.

(61) Corma, A.; Renz, M. Water-Resistant Lewis-Acid Sites: Carbonyl-Ene Reactions Catalyzed by Tin-Containing, Hydrophobic Molecular Sieves. *ARKIVOC* **2006**, *2007*, 40.

(62) Tan, J. Z.; Bregante, D. T.; Torres, C.; Flaherty, D. W. Transition State Stabilization Depends on Solvent Identity, Pore Size, and Hydrophilicity for Epoxidations in Zeolites. *J. Catal.* **2022**, *405*, 91−104.

(63) Potts, D. S.; Jeyaraj, V. S.; Kwon, O.; Ghosh, R.; Mironenko, A. V.; Flaherty, D. W. Effect of Interactions between Alkyl Chains and Solvent Structures on Lewis Acid Catalyzed Epoxidations. *ACS Catal.* **2022**, *12*, 13372−13393.

(64) Corma, A.; García, H. Lewis Acids: From Conventional Homogeneous to Green Homogeneous and Heterogeneous Catalysis. *Chem. Rev.* **2003**, *103*, 4307−4366.

(65) Prodinger, S.; Derewinski, M. A. Recent Progress to Understand and Improve Zeolite Stability in the Aqueous Medium. *Petrol. Chem.* **2020**, *60*, 420−436.

(66) Román-Leshkov, Y.; Moliner, M.; Labinger, J. A.; Davis, M. E. Mechanism of Glucose Isomerization Using a Solid Lewis Acid Catalyst in Water. *Angew. Chem.* **2010**, *122*, 9138−9141.